Materials Today Bio 27 (2024) 101152

Contents lists available at ScienceDirect

Materials Today Bio

journal homepage: www.journals.elsevier.com/materials-today-bio

Impact of uniaxial cyclic stretching on matrix-associated endothelial cell responses

Cuihong Ren [a,b], Zhonghua Chang [c], Kecheng Li [a,b], Xiaofeng Wang [a,b,*], Dongfang Wang [a,b], Yiyang Xu [b], Xiaomeng Li [a,b], Qian Li [a,b,*]

[a] School of Mechanics and Safety Engineering, Zhengzhou University, Zhengzhou, 450001, PR China
[b] National Center for International Research of Micro-Nano Molding Technology, Zhengzhou University, Zhengzhou, 450001, PR China
[c] Institute of Laser Manufacturing, Henan Academy of Sciences, Zhengzhou, 450046, PR China

ARTICLE INFO

Keywords:
Uniaxial cyclic stretching
Matrix morphology
Endothelial nitric oxide (NO) release

ABSTRACT

Uniaxial cyclic stretching plays a pivotal role in the fields of tissue engineering and regenerative medicine, influencing cell behaviors and functionality based on physical properties, including matrix morphology and mechanical stimuli. This study delves into the response of endothelial cells to uniaxial cyclic strain within the geometric constraints of micro-nano fibers. Various structural scaffold forms of poly(L-lactide-*co*-caprolactone) (PLCL), such as flat membranes, randomly oriented fiber membranes, and aligned fiber membranes, were fabricated through solvent casting and electrospinning methods. Our investigation focuses on the morphological variation of endothelial cells under diverse geometric constraints and the mechanical-dependent release of nitric oxide (NO) on oriented fibrous membranes. Our results indicate that while uniaxial cyclic stretching promotes endothelial cell spreading, the anisotropy of the matrix morphology remains the primary driving factor for cell alignment. Additionally, uniaxial cyclic stretching significantly enhances NO release, with a notably stronger effect correlated to the increasing strain amplitude. Importantly, this study reveals that uniaxial cyclic stretching enhances the mRNA expression of key proteins, including talin, vinculin, rac, and nitric oxide synthase (eNOS).

1. Introduction

Tissue engineering scaffolds serve as a favourable extracellular matrix (ECM) environment for cell processes, experiencing intricate external mechanical forces during tissue repair and regeneration cycles [1]. Cellular responsiveness to mechanical signals governs fundamental cellular behaviors such as adhesion, proliferation, migration, apoptosis, and differentiation [2]. Understanding these responsive behaviors aids in predicting cell fate, unraveling disease mechanisms, and guiding the design of tissue engineering scaffolds [3]. Within vascular tissue engineering, mechanical forces encompass shear forces from blood flow and radial cyclic stretching forces induced by cardiac pulsations, with uniaxial cyclic stretching emerging as a critical regulator of endothelial cell (EC) morphology and function [4,5].

In physiological conditions, such as processes like cardiac cycles and respiration, endothelial cells exhibit precise sensitivity to dynamic uniaxial stretching of the underlying substrate [6], leading to distinctive morphological reorientations [7–9]. This response involves subcellular changes, including cytoskeleton reorientation [10,11] and internal contractile forces [12], influencing cell function, particularly in endothelial cell-dependent nitric oxide (NO) release [13], and this effect varies with the stretching frequency [14] and strain amplitude [15–17]. While previous studies have explored the effects of cyclic stretching on isotropic plane polydimethylsiloxane (PDMS) elastic membranes [18], limited knowledge exists regarding the response of endothelial cells on vascular tissue engineering scaffolds to cyclic stretching.

Electrospun poly(L-lactide-*co*-caprolactone) (PLCL) vascular scaffolds offer customizable topological structures and controlled mechanical properties. Previous research has successfully demonstrated tissue remodeling with these scaffolds in small-caliber applications [19],[22]. Moreover, investigating the impact of cyclic stretching on endothelial cell morphology and functionality on diverse vascular scaffold substrates is crucial for scaffold design and understanding matrix-cell responses to cyclic stretching.

In this study, we employed electrospinning technology to prepare vascular tissue engineering scaffolds with micro-nano fibrous structures,

* Corresponding authors. School of Mechanics and Safety Engineering, Zhengzhou University, Zhengzhou, 450001, PR China.
E-mail addresses: ren_cuihong@126.com (C. Ren), 991157540@qq.com (Z. Chang), 13525998834@163.com (K. Li), xiaofengwang@zzu.edu.cn (X. Wang), wang.17@outlook.com (D. Wang), 1070072867@qq.com (Y. Xu), xiaomeng.li@zzu.edu.cn (X. Li), qianli@zzu.edu.cn (Q. Li).

https://doi.org/10.1016/j.mtbio.2024.101152
Received 9 April 2024; Received in revised form 7 June 2024; Accepted 8 July 2024
Available online 9 July 2024

in both disordered and oriented arrangements. Flat scaffolds were fabricated by casting served as a control group. We explored the response of endothelial cells to cyclic stretching on various scaffold topologies, revealing that cells tended to align perpendicular to the stretching direction; anisotropic topological structures predominantly guided morphology. Notably, functional endothelial cells exhibited positively regulated nitric oxide release in response to cyclic stretching frequency and strain magnitude.

2. Materials and methods

2.1. Materials

PLCL (intrinsic viscosity = 3.2 dlg^{-1}) was purchased from Jinan Daigang Biotechnology Co., Ltd (Jinan, China). SYLGARD™ 184 Silicone Elastomer Kit came from Dow Corning. Dichloromethane (DCM) and N, N dimethylformamide (DMF) were bought by Tianjin Kemiou Chemical Co., Ltd (Tianjin, China). Syringe Propulsion Pump (LSP02-2A) was purchased from Baoding Longerpump Co., Ltd (Baoding, China). HUVECs (human umbilical vein endothelium cells) were purchased from Beijing Oligobio. RPMI DEME, PBS, and fetal bovine serum were purchased from BI. CCK8 assay was purchased from Japanese Dojindo. Live/Dead Viability Kit was purchased from KeyGEN BioTECH. CF 568 phalloidin, 4′,6-diamidino-2-phenylindole (DAPI), and ananti-vinculin antibody were bought from Biotium, Beyotime, and Abcam, respectively. Fluorescent probe 4-amino-5-methylamino-2′, 7′-difluorofluorescein diacetate (DAF-FM DA) and Total Nitric Oxide Assay Kit were purchased from Beyotime Biotechnology (Shanghai, China).

2.2. Build mechanical Cyclic Stretching Device

The uniaxial cyclic stretching structure consisted of three main components: a deformable PDMS culture chamber (Fig. 1a), a loading device (Fig. 1b), and a ball screw reciprocating feeding system (Fig. 1c). The PDMS culture chamber was fabricated by pouring a mixture of base material and curing agent (Sylgard 184 silicone elastomer kit) in a 10:1 wt ratio. The fabrication process involved mixing, degassing, curing, and demolding, with a curing temperature of 70 °C for 12 hours. To prevent slippage, friction-enhancing grooves (Fig. 1d) in a pattern resembling anti-slip tape were added to the contact area with the lid. The culture chamber was firmly fixed in the groove of the fixing device, and the other end connected to the feeding system through a ball screw. The feeding system is driven by a stepper motor (DQ-42HB60A) (Fig. 1e), which receives specific instructions from a servo motor controller (KH-01). This arrangement enables the implementation of various modes of uniaxial cyclic stretching.

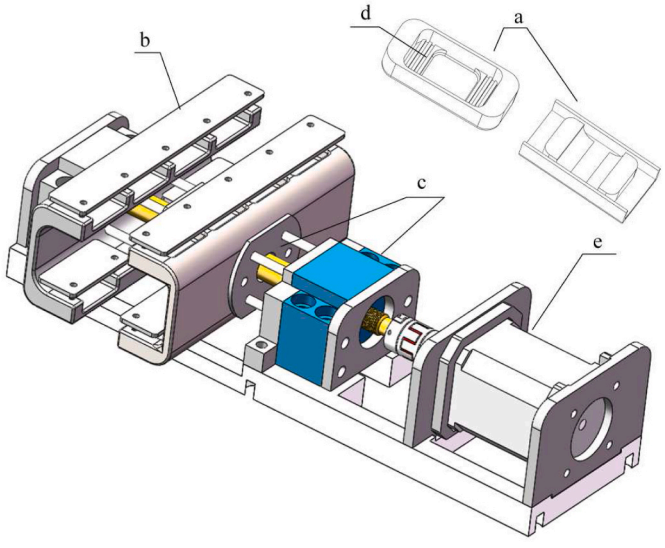

Fig. 1. Cyclic Stretching Device. a) Deformable polydimethylsiloxane (PDMS) culture chamber. b) Loading device. c) Ball screw reciprocating feeding system. d) Friction-enhancing grooves. e) Stepper motor.

2.3. Preparation of samples with different matrix morphology

Micro/nanofiber membranes were fabricated by the electrospinning technique and named as 'Random' and 'Align', respectively. To prepare these membranes, 0.8 g of PLCL was dissolved in a mixture of 10 ml of DCM and DMF (in a volume ratio of 7:3). The solution was delivered at a rate of 2 ml/h using a syringe pump through an 18 G stainless steel needle (with inner diameter of 0.9 mm and outer diameter of 1.26 mm). The electrospinning setup was configured with a high-voltage power supply set to 18 kV and a negative pressure of -0.2 kV, with a working distance of 16 cm. The flat samples, designated as 'Flat', were created by pouring a solution of 6 % PLCL in DCM. The resulting membranes had a uniform thickness of 0.035 ± 0.005 mm. Finally, these membranes were cut into rectangular shapes measuring 1*4 cm.

2.4. Characterising the physical properties of samples

Scanning electron microscope (SEM): After sputtering a thin layer of platinum onto the samples, FEI Quanta 250 FEG were applied to capture the images at an accelerating voltage of 10 kV. Subsequently, software of ImageJ software and Fast Fourier Transform (FFT) [23] analysis were employed to statistically analyze the diameter distribution and fiber orientation of the samples.

Atomic Force Microscope (AFM): Matrix morphology and surface roughness of the samples were examined by an AFM (Keysight 8500, U. S.A) in tapping mode. The testing area covered a 20*20 μm region with a scan rate of 0.80 lines/second. The experiments were carried out in air at room temperature, and the AFM images were processed and analyzed using Pico Image Basic 7.2 software.

Water Contact Angle: Wetting properties of the samples were assessed using a camera (JC2000D1, China Zhongchen Corporation). Four samples were tested for each group, with three measurements taken on each sample. At room temperature, 2 μL of deionized water was dispensed onto the surface of the fiber membrane.

2.5. Mechanical test

Uniaxial Tensile Testing: An electronic universal testing machine (UTM2230, manufactured by SUNS Technology Company, Shenzhen, China) was employed. The testing parameters were set as follows: a testing speed of 5 mm per minute and a load of 100 N, all conducted at room temperature (23 °C). The tensile direction of Align group was consistent with the fiber arrangement. To assess the mechanical stability of the samples before and after the tensile tests, cyclic loading was applied to both the control (unstretched) and stretched groups of samples. Subsequently, stress-strain curves were generated and analyzed using software of Origin 8.5.

Nanoindentation: To characterize the surface stiffness of the samples, nanoindentation was performed by a spherical-tipped nanoindenter (Agilent Technologies G200). The depth was maintained at 5000 nm in each displacement-controlled mode. Subsequently, data analysis was carried out using software of Origin 8.5 and GraphPad 8.0.

2.6. Culturing and in vitro cycling stretching of HUVECs

Cell culture procedures were conducted following our prior work [24], with a modification to the culture medium, which was replaced with DMEM containing 10 % bovine serum albumin. Prior to use, culture dishes were soaked in alcohol for 2 hours and subjected to 10 min of UV irradiation. Each group of samples was seeded with cells from the same

passage at a density of 5000 cells/cm^2, with the seeding area located at the center of rectangular samples. Following seeding, media were changed every 24 hours. After three days of culture, half of the cell-seeded samples were transferred to the PDMS culture chamber and subjected to uniaxial periodic stretching stimulation, while the other half was cultured statically (as a control). The culture device and samples were placed in an incubator at 37 °C for 24 hours. The stretching parameters were set at 1 Hz, (10 %, 15 %, 20 %), and 10 % (0.8 Hz, 1 Hz, 1.2 Hz). The frequency and amplitude of the stretching are set based on the normal physiological condition [25].

2.7. Immunostaining assessment of cells

Cell viability: Cell viability on day 1, day 3 and day 4 in static and dynamic conditions was determined using the Live/Dead Cell Viability/Cytotoxicity Assay Kit (KeyGEN BioTECH). AM (Calcein Acetoxymethyl Ester) and PI (Propidium Iodide) were employed to label live and dead cells, respectively. AM can penetrate the cell membrane of living cells and produce green fluorescent substance with strong fluorescent signal in the presence of esterase activity; PI can penetrate the cell membrane of damaged or dead cells and bind to nucleic acids with red fluorescent signal. Incubate for 30 minutes at room temperature, wash the samples with PBS and observe the imaging under a confocal microscope (LSM 880, Zeiss, Germany).

Proliferation: Cell proliferation was assessed on days 1, 3, and 4 of cell culture using the CCK-8 cell counting kit. CCK8 (20 μL) dissolved in 200 μL of medium was used as the assay solution for each sample, and six replicate samples were added to the assay solution and incubated at 5 % CO2 and 37 °C for 2 hours. Subsequently, 100 μL of medium containing CCK8 was drawn and added to the 96-well plate. The absorbance was measured at 450 nm using an enzyme marker and the cell number was calculated. The seeding density for each sample was 5000 cells/cm^2.

Morphology: Cell morphology was visualized by staining with DAPI, CF 568 Phalloidin, and anti-vinculin antibody. Cells were fixed with 4 % formaldehyde for 10 min and permeabilised with 0.1 % BSA/10 % normal goat serum/0.3 M glycine in 0.1 % PBSTween. Immediately thereafter, cells were permeabilised with 0.1 % BSA/10 % normal goat serum/0.3 M glycine in 0.1 % PBST for 1 hour and then washed with 1 % BSA in PBST. Finally, cells were incubated overnight at 4 °C with anti-zinc protein antibody dilution (1:50v:v dilution, 1 % BSA) (green). Label nuclear DNA (blue) with DAPI. Repeat the above fixation to closure, then incubate the cells with rabbit primary antibody (anti-vinculin) overnight, then rinse with PBS and repeat three times. Finally, the cells were labelled with CoraLite488-conjugated Afffinipure goat anti-rabbit protein for 1 hour at room temperature, 20 min and then 10 min with DAPI. The skeleton and vinculin samples obtained above were imaged with a laser scanning confocal microscope (LSM 880, Zeiss, Germany).

2.8. Statistical parameters of cell morphology

Stress Fiber Orientation Analysis: We assessed the orientation of stress fibers in HUVECs stained with myosin immunofluorescence using Image J [26]. The orientation of stress fibers was determined in relation to the x-axis of the images, which also represents the direction of strain. To ensure accurate analysis, the fluorescence images of the fibers were first processed using Fiji. This involved background subtraction and contrast enhancement to enhance the quality of the images. Subsequently, we employed the Directionality plugin (http://fiji.sc/wiki/index.php/Directionality) to conduct a detailed directional analysis of stress fibers. This analysis included the measurement of peak positions achieved through Gaussian fitting of the Fast Fourier Transform (FFT) signal, providing valuable data on the orientation of stress fibers.

Nuclear Shape Index (NSI) and Nuclear Aspect Ratio Calculation: The long and short axes of cell nuclei were quantified by employing an image-based elliptical fitting method. Subsequently, NSI was calculated using Equation (1)[27], and the nuclear aspect ratio was determined using Equation (2) :

$$\mathrm{NSI} = \frac{4\pi \times \mathrm{area}}{\mathrm{perimeter}^2} \tag{1}$$

$$\text{Nuclear Aspect Ratio} = \frac{L_N}{W_N} \tag{2}$$

where LN and LW are half of the nuclear length and nuclear width, respectively.

Circularity and Cell Aspect Ratio Calculation: Cell long and short axes, as well as spreading area and perimeter, were quantified using an image-based elliptical fitting approach. Circularity was subsequently computed using Equation (3), and cell aspect ratio was determined using Equation (4)[28].

$$\text{Circularity} = \frac{4\pi \times \text{spreading area}}{\text{perimeter}^2} \tag{3}$$

$$\text{Cell Aspect Ratio} = \frac{L_C}{W_C} \tag{4}$$

where L_C and W_C are the long and short cell diameters, respectively.

2.9. Measuring nitric oxide release

Adjusting the concentration of the nitric oxide fluorescent probe (DAF-FM DA) to 5 μM, the samples were incubated at 37 °C for 60 min. The staining solution was then aspirated, followed by three slow washes with deionized water, each lasting 5 min. Subsequently, confocal microscopy imaging was performed.

Determination of NO concentration：using the NO assay kit, 60 μL of cell culture supernatant was transferred to a 96-well plate. Next, 5 μL of NADPH, 10 μL of FAD, and 5 μL of Nitrate Reductase were sequentially added, and the mixture was incubated at 37 °C for 30 min. The purpose of this step was to reduce nitrates to nitrites. Following this, 10 μL of LDH buffer and 10 μL of LDH were added to neutralize the impact of NADPH. Finally, 50 μL of Griess Reagent I and 50 μL of Griess Reagent II were added to measure the total amount of nitrites converted from nitrates, allowing for the inference of NO production based on a standard curve. NO release data were normalized to CCK-8 data using normalization formula (5).

$$\text{stretched/unstretched ratio of NO release} = \frac{\left(\frac{OD_{NO\ release}}{OD_{cck-8}}\right)_{\text{stretched}}}{\left(\frac{OD_{NO\ release}}{OD_{cck-8}}\right)_{\text{unstretched}}} \tag{5}$$

2.10. Total RNA extraction and quantitative polymerase chain reaction analysis

We utilized quantitative real-time Quantitative polymerase chain reaction (qRT-PCR) to assess the expression of relevant genes. RNA extraction was carried out using TRIzol reagent (Thermo Fisher), followed by cDNA synthesis using the RevertAid First Strand cDNA Synthesis Kit (Thermo Fisher) to obtain complementary DNA (cDNA). The relative expression levels of the target genes were analyzed using the PowerUp SYBR Green Master Mix (Thermo Fisher). Detailed experimental procedures can be found in previous work [29](Table S2).

2.11. Statistical analyses

Unless otherwise specified, all experiments were conducted a minimum of three times ($n > 3$ or $n = 3$). One-way analysis of variance (ANOVA) was employed to assess significant differences among three or more groups, while the *t*-test was used to analyze significant differences

between two groups. A significance threshold of *P < 0.05, **P < 0.01, and ***P < 0.001 was considered statistically significant. Standard deviation is depicted as error bars. All data are presented as mean ± standard deviation.

3. Results

3.1. Surface morphology of the three different substrates

To investigate the behavior of endothelial cells on different orientations of micro/nanofiber scaffolds under uniaxial cyclic stretching, we prepared PLCL samples in the form of flat films, random fiber films, and aligned fiber films. Flat samples were fabricated using a solvent casting method, while random and aligned micro/nanofiber films were prepared via electrospinning. Fig. 2 shows the SEM (Fig. 2A) and AFM (Fig. 2B) images, and these images revealed the different microscale surface structures of the three types of samples: the Flat group exhibited a smooth surface, whereas the surfaces of the Random and Align groups were characterized by smooth and relatively uniform fibers. AFM images of the Flat group exhibited subtle textures attributed to solvent flow during the casting process. However, there were no significant differences in the surface roughness among these three sample groups. Statistical analysis of fiber diameters (Fig. 3A) showed that the fibers in the Random group had a diameter of 1.06 ± 0.223 μm, while those in the Align group had a diameter of 1.19 ± 0.274 μm. Hence, we can disregard the influence of diameter on cell behavior.

The results of FFT (Fig. 3B) fiber orientation analysis indicated that fibers in the Random group exhibited smaller fluctuations but a uniform distribution, signifying even distribution at 180°. In contrast, the Align group's fibers displayed a shark peak at 90°, indicating a superior fiber orientation [23]. The water contact angle results indicated that the Random and Align groups had no significant difference, but both are higher than the flat group (Fig. S1).

3.2. Mechanical Behaviour of the scaffold

To eliminate the influence of surface mechanics properties on cell behavior and functionality, we conducted stiffness measurements using a nanoindentation instrument. The results (Fig. 4A–B) revealed that compared to flat films with a stiffness of approximately 6 MPa, the fiber-based samples exhibited higher stiffness, approximately 25 MPa. All three groups exhibited values in the range of 6–25 MPa, which exceeds the stiffness range typically sensed by cells in ECM (1–100 kPa) [30].

To reflect the circumstance in vivo, we simulated the morphological responses of cells at a frequency of 1 Hz [31,32] and under strain amplitude of 10 %. We also investigated variations in cellular function, specifically NO release, under strain amplitudes of 10 %, 15 %, and 20 % in the oriented fiber group. Mechanical curves for the control (unstretched) and stretched samples of the three groups were obtained through uniaxial cyclic stretching (Fig. 5). The results indicated a high degree of overlap in the cyclic stretching curves between the two groups, with the stretched group exhibiting slightly lower tensile strength (Table S1). Under strain conditions of 10 % and 15 %, all three groups displayed almost linear stress-strain behavior, while at 20 % strain, the response was nonlinear.

In particular, after the initial tensile cycle, the stress required for all groups at the same strain amplitude is reduced, a phenomenon known as stress softening, akin to the Mullins effect [23]. This phenomenon is reminiscent of the mechanical behavior observed in various tissues, particularly in blood vessels [33].

3.3. HUVECs activity and proliferation

In this investigation, the biocompatibility of PLCL samples was systematically evaluated, as depicted in Fig. 6. Live and dead cells were distinguished utilizing AM and PI, respectively. Cell viability and proliferation were quantified through the CCK-8 assay. The results showed that the number of cells on random and aligned fiber membranes was significantly higher than that on planar membranes on day 4. Conversely, the cell count decreased in all groups following the stretching treatment. Nevertheless, it is noteworthy that the cell viability of all samples were above 90 %. Moreover, the cell proliferation curves (Fig. S2) displayed exponential characteristics, indicating a robust cellular response to the PLCL samples under assessment.

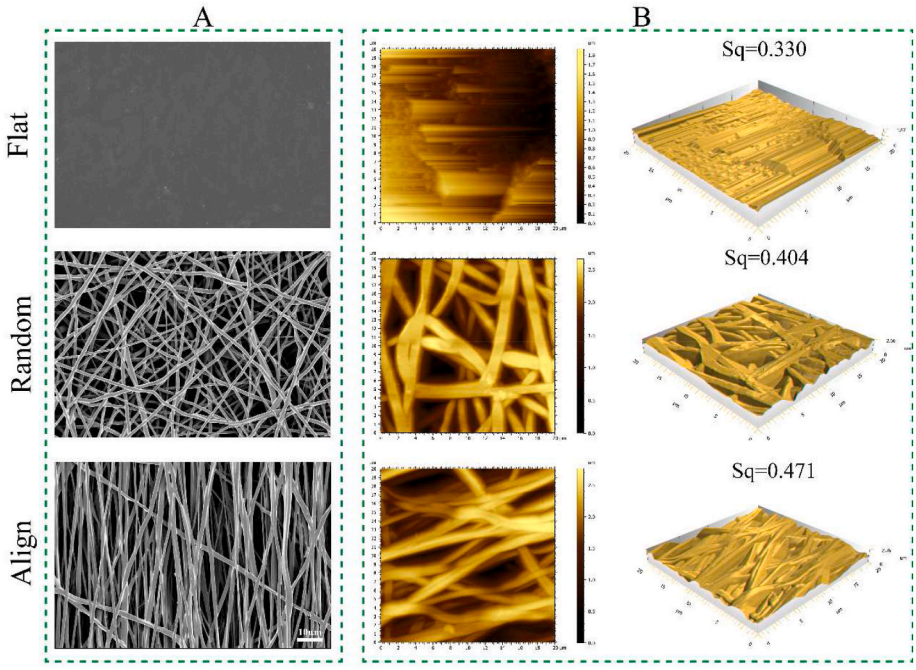

Fig. 2. Distribution of surface morphology. A) Scanning electron microscope images of 'Flat', 'Random' and 'Align'. B) Atomic force microscope images of 'Flat', 'Random' and 'Align'. The unit of Sq is um.

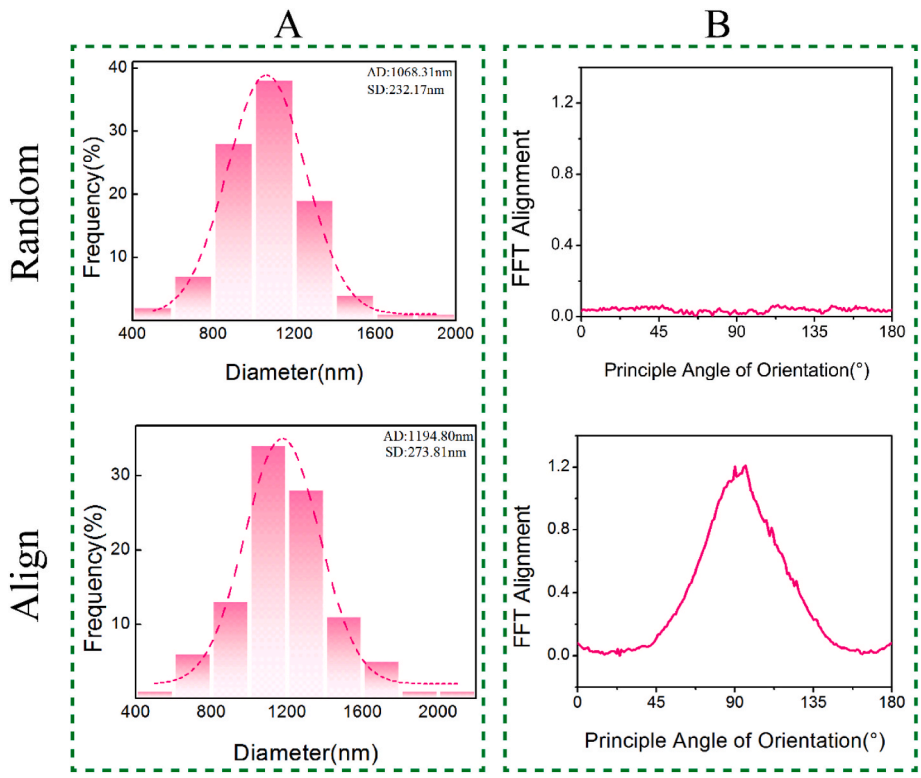

Fig. 3. Statistical analysis of fiber diameters and the results of fast Fourier transform. A) fiber diameters images of Random and Align. B) fast Fourier transform (FFT) images of Random and Align.

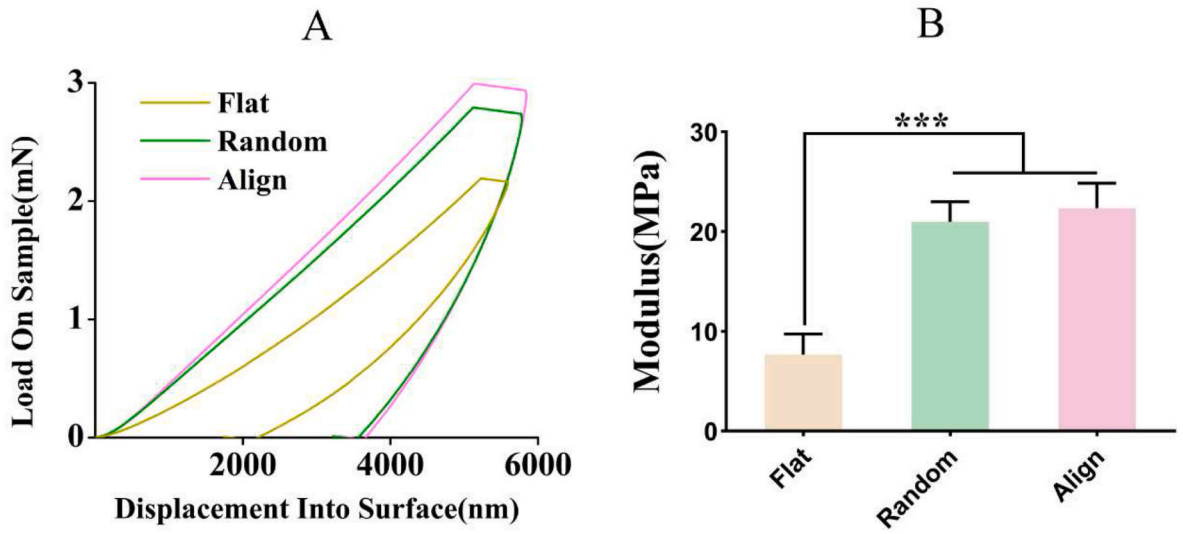

Fig. 4. Nanoindentation images A) Nanometer indentation displacement−load diagram B) Elastic modulus of different surface topography samples.

3.4. Cyclic stretching changes cell morphology

Cell morphology variation with cyclic stretching was observed through immunofluorescence staining results (Fig. 7). On Day 4, cells on flat membranes are a nearly circular shape, attributed to the uniform isotropic guides along the cell boundaries. Whereas cells on random fiber membranes have a cobblestone-like boundary, and cells on aligned fiber membranes appear spindle-shaped, as the fibers provided specific anchoring points in certain directions. However, after undergoing stimulation of stretching for 24 hours, the overall cell spreading area increased (Fig. 8B). By fitting cell shapes with ellipses, we observed changes in cell polarization (Fig. 8A). Specifically, the cell polarization of the Flat and Random groups significantly increased after receiving uniaxial cyclic stretching stimulation, while the cell polarization of Align group was weakened by mechanical stimulation. Reduction in cell circularity (Fig. 8C) primarily occurred in the Random group, while the cell circularity in the Flat and Align groups did not exhibit significant variations.

As one of the largest and structurally resilient organelles within cells, the cell nucleus serves as a recipient of forces exerted by the cellular cytoskeleton [34] and also dynamically adapts its shape in response to mechanical cues [35]. The evaluation of nuclear morphology indices,

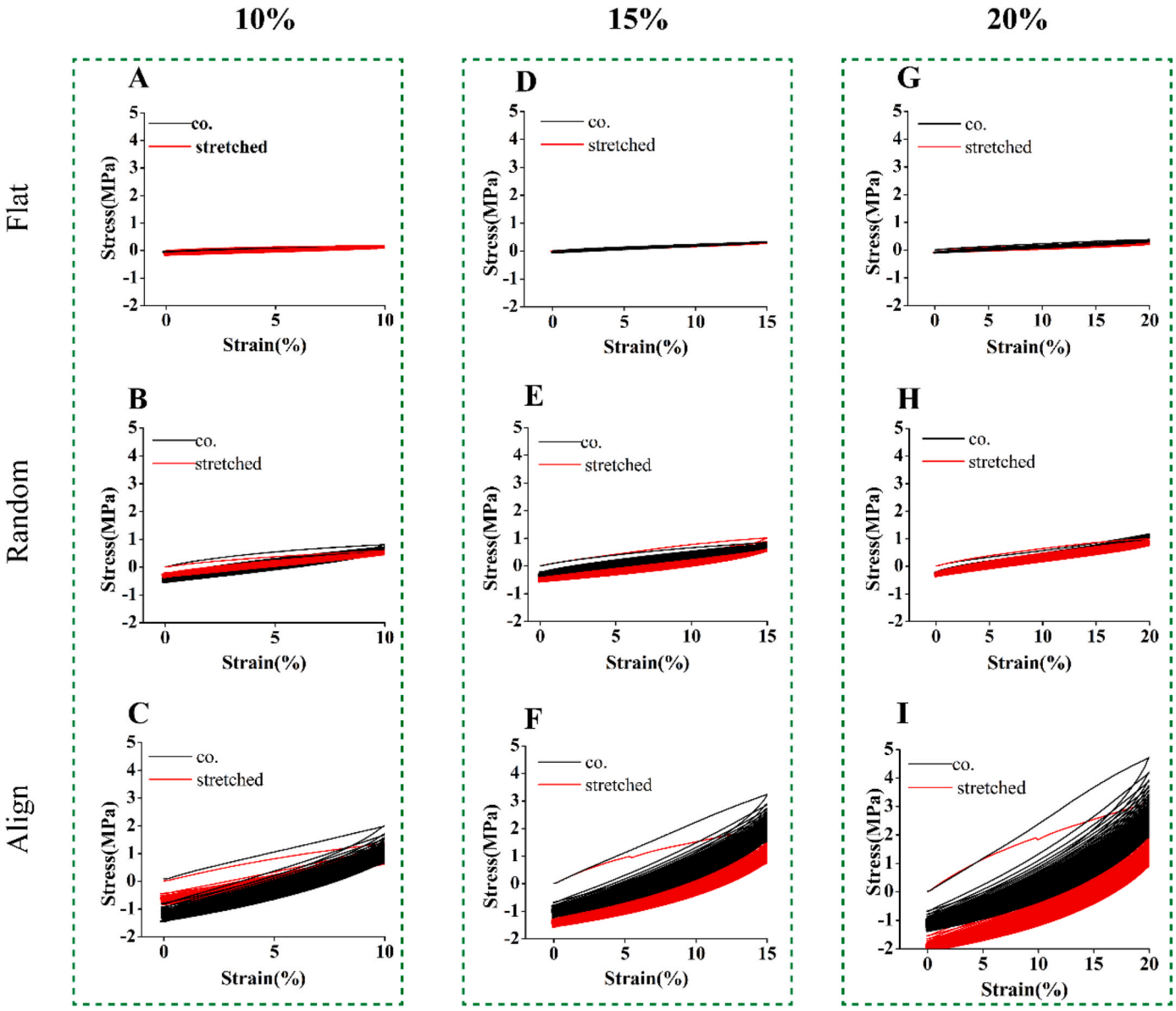

Fig. 5. Stresses and strains curves of uniaxial Tensile Testing. A-C) 10 % strain. D-F) 15 %. G-I) 20 % strain.

specifically the Nuclear aspect ratio (Fig. 8E) and the NSI (Fig. 8F), revealed noteworthy observations. Notably, a significant increase in nuclear morphology index was observed in both the Flat and Align groups, indicative of alterations in nuclear shape under specific mechanical conditions. Conversely, the Random group showed no significant changes in the nuclear morphology index. Interestingly, the aspect ratio of cell nuclei did not demonstrate significant changes across all the experimental groups. These findings provide insights into the mechanical modulation of nuclear morphology and highlight distinct responses in different experimental conditions.

Stress fiber distributions, as assessed through immunofluorescence, were scrutinized for fiber orientation in both control (unstretched) and stretched groups (Fig. 7A–C). Under unstretched conditions on Day 4, the cells in the Flat and Random groups exhibited a subtle orientation, predominantly distributed uniformly around 180°. In contrast, the cells in the Align group displayed a highly oriented distribution along the direction of the fibers, aligning with the strain direction. Following 24 hours of stretching, the changes in the orientation direction of the stress fibers in the three groups were observed. The Flat group experienced a rotational shift, transitioning from approximately -10° to around -50° (Fig. 7A), rather than rotating a full 90°. This might be attributed to the material's Poisson's ratio, which is 4 % for the two-dimensional membrane used in the test. Consequently, when the membrane is subjected to longitudinal stretching, it simultaneously encounters compressive forces in the perpendicular direction, possibly restricting its rotation. Calculations suggest that cells rotate approximately 55° towards the direction. Conversely, the angles in the "Random" and "Align" groups remained stable approximately -40° and -30°, respectively, with no alteration in the primary orientation direction (Fig. 7 B, C). The difference lies in that under the guidance of aligned fibers, the reorganization of cellular stress fibers perpendicular to the direction of strain is constrained by geometric shapes, manifesting only as a widening in the orientation distribution of stress fibers and an increase in the adhesion area at the cell borders. In contrast, on random fiber membranes, cells are subjected to forces in directions from 0 to 90°, with the maximum strain occurring in the direction of maximum strain (0°). Stress fibers are reorganized to avoid the impact of the maximum strain direction and are compressed by the forces perpendicular to the direction of strain, with a resultant force forming a directional peak around 40°. The observation underscores that cells align with fiber orientation, and uniaxial cyclic

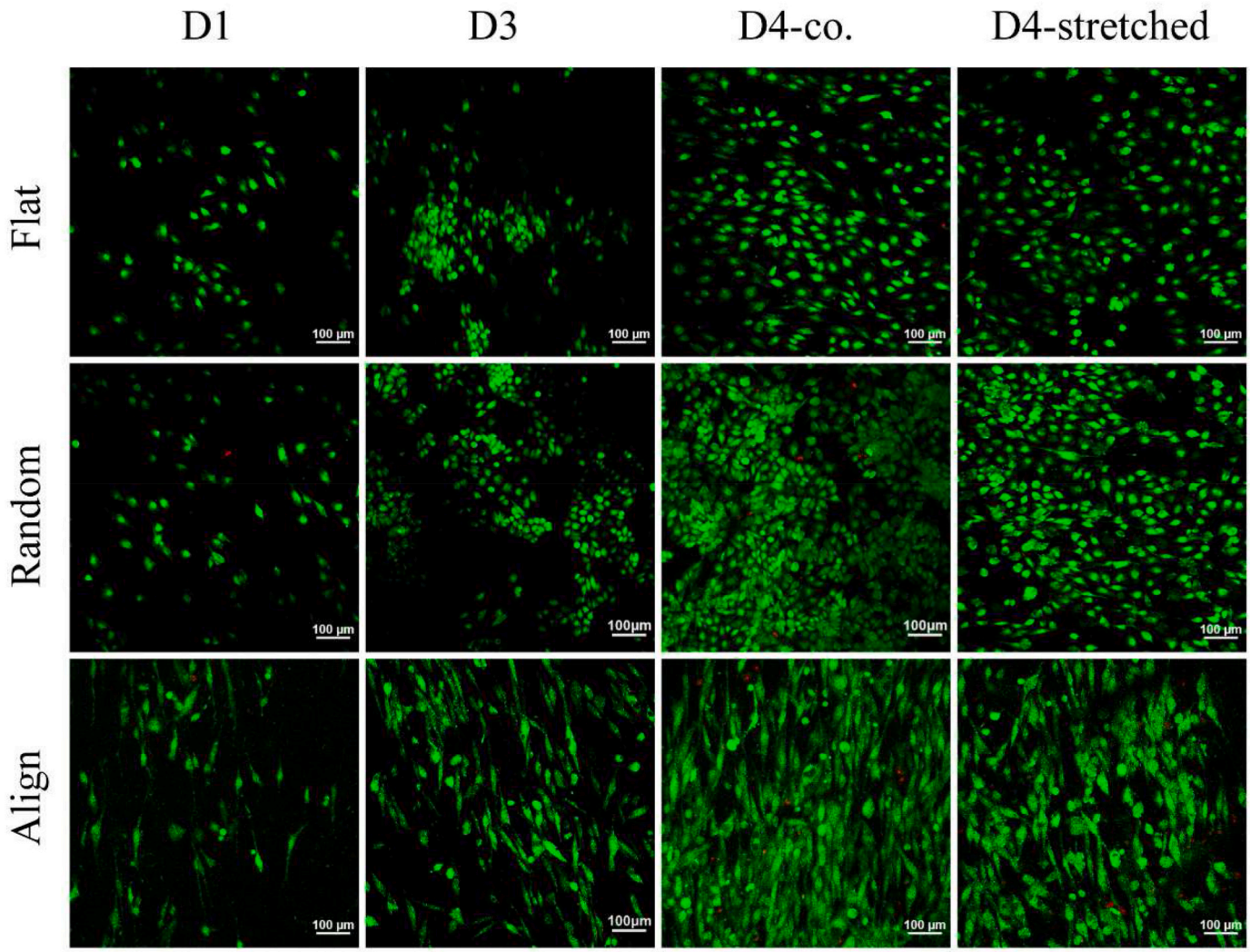

Fig. 6. Live–dead staining of HUVECs of different groups on day 1, day 3, day 4 (the scale bar is 100 μm), (Co. represents unstretched).

stretching also does not induce significant changes in the main orientation. Essentially, cell orientation is primarily influenced by matrix fiber morphology cues initiated by contact-induced interactions [36].

3.5. NO release enhanced by cyclic stretching

Beyond its impact on cell morphology, uniaxial cyclic mechanical stretching exerts regulatory control over cellular functions. NO, a soluble functional molecule secreted by endothelial cells, plays a pivotal role in governing various physiological processes, including cardiovascular function, metabolism, neural transmission and immune response [37]. Previous investigation, both in vitro and in vivo, have demonstrated a significant elevation in nitric oxide release in response to mechanical stretching stimuli [38]. To further understand the mechanism behind this change, we explored the changes in NO release when subjected to mechanical stretch and performed changes in nitric oxide synthase (eNOS) mRNA, which is critical for elucidating the kinetics of NO release. Given that stretching did not alter the direction of cell polarization by matrix morphology, with the least change observed in the Align group, this group was selected for studying NO release. This choice aims to isolate, to the greatest extent possible, the influence of morphology changes on NO release.

Pre- and post-mechanical stimulation assessments revealed a significant augmentation in DAF-FM staining (Fig. 9A), signifying that 1Hz, 10 % cyclic stretching induces the release of NO in endothelial cells. This observation was further substantiated through rigorous statistical analysis (Fig. 9B), establishing a positively regulatory effect of cyclic stretching on endothelial-dependent NO release [39,40].

Subsequently, a detailed exploration was conducted to elucidate the correlation between NO release and both strain amplitude and strain frequency. HUVECs were cultured on oriented fibers and subjected to tensile strains of 10 %, 15 %, and 20 % (Fig. 9D), and strain frequencies of 0.8 Hz, 1 Hz, and 1.2 Hz (Fig. 9C) for a duration of 24 h. Following this, NO release levels were normalized (Formula 5). The results reveal a positive correlation between NO release and both strain amplitude as well as frequency, with a notable emphasis on the pronounced dependence on strain frequency.

3.6. Expression of genes versus cellular mechanosensing factors

Alterations in cell morphology serve as external manifestations of intricate internal biochemical signal transduction processes [41]. To decipher how cells perceive uniaxial cyclic stretching from the ECM, we conducted an assessment of changes in the gene expression of mechanical sensors known to actively engage in mechanical signal transduction. This approach contributes to a more comprehensive understanding of cell perception of mechanical stimuli from the perspective of signal transduction pathways. The examined mechanical

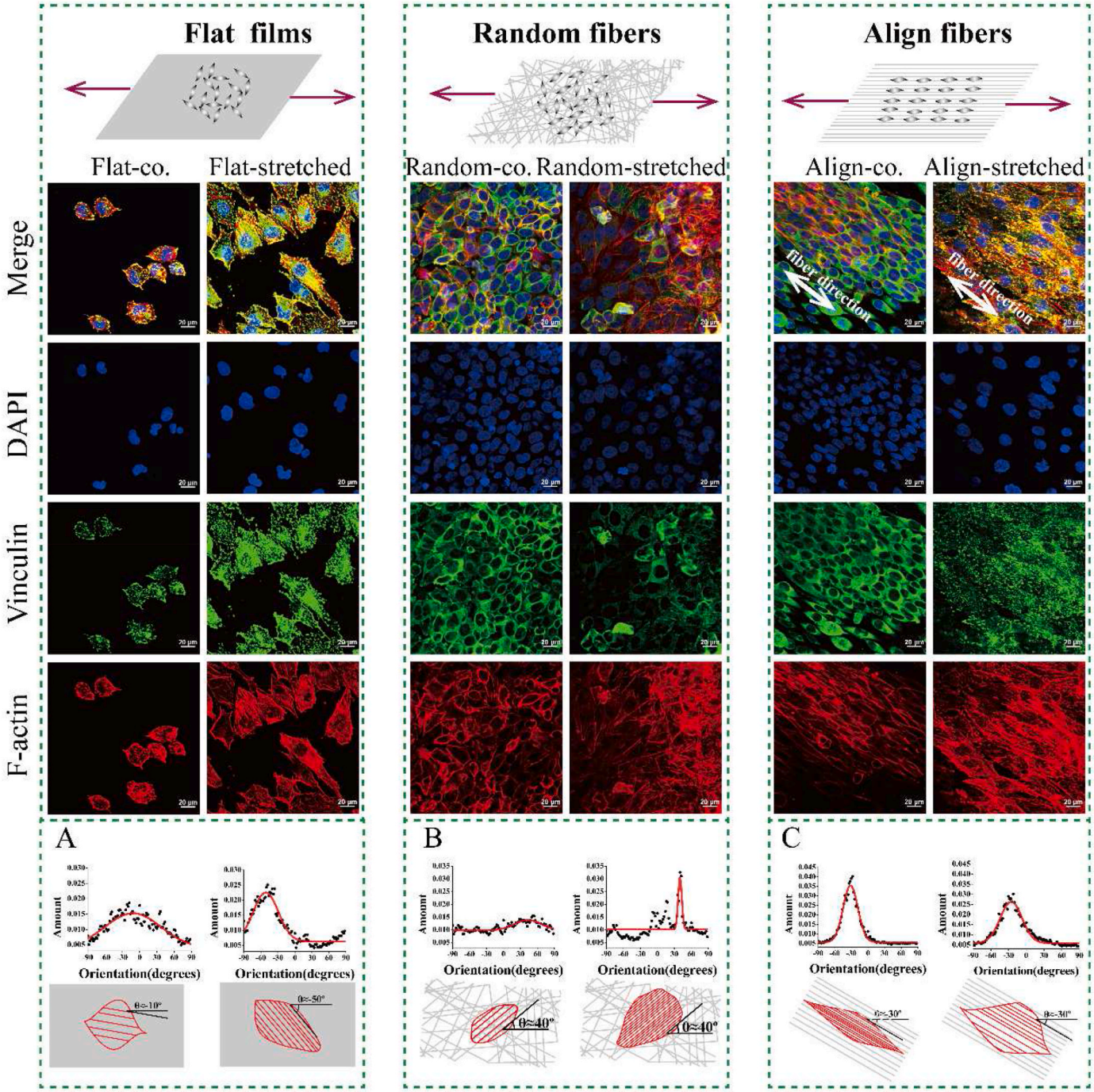

Fig. 7. Immunofluorescence staining of HUVECs cultured in different groups under co. (unstretched) and stretched conditions (scale bar 20 μm). A-C) Stress fiber orientation of HUVECs cultured in different groups under co. (unstretched) and stretched conditions (scale bar 20 μm).

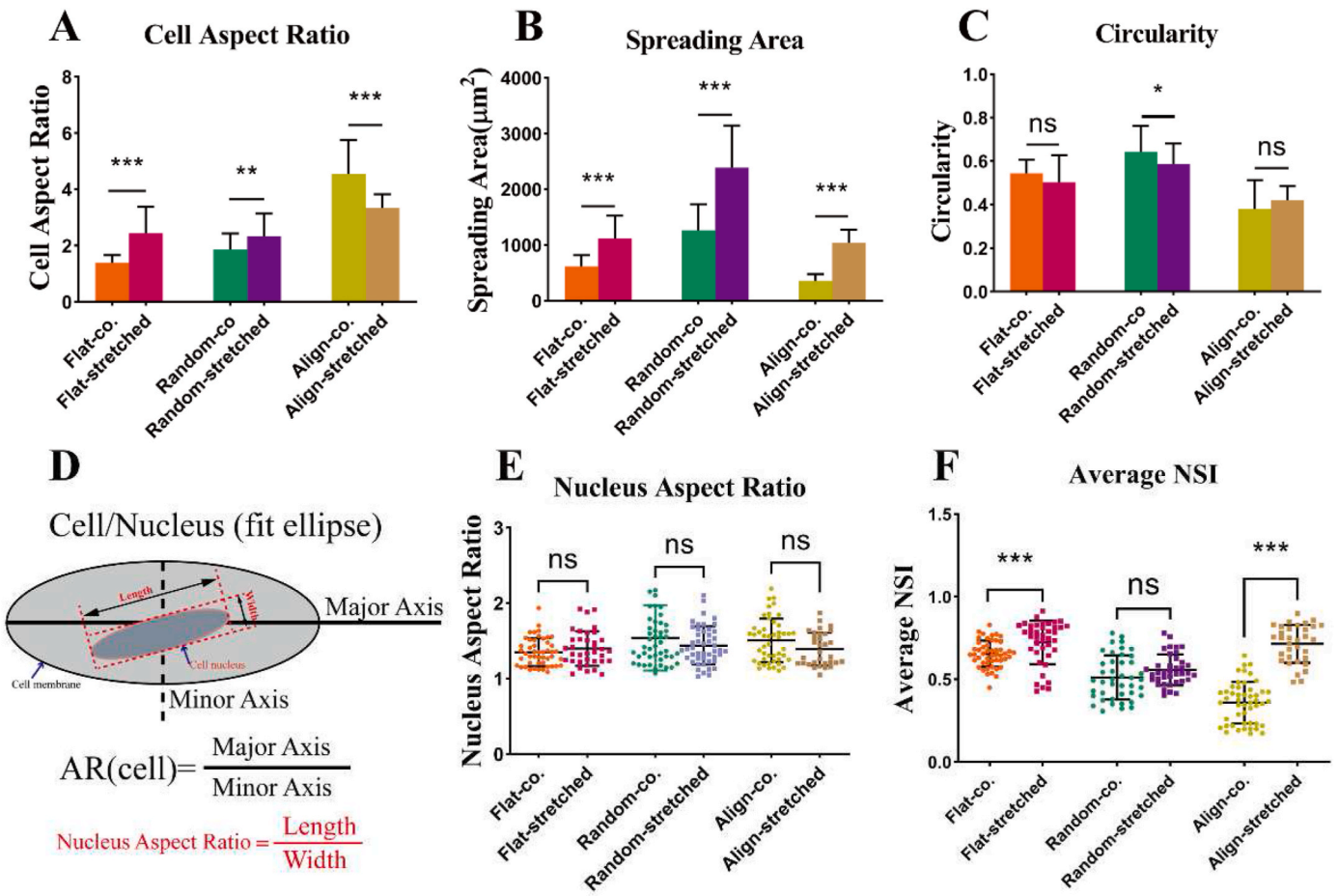

Fig. 8. Statistical graphs of immunofluorescence (A, C) Cell polarization was evaluated by cell aspect ratio and circularity, respectively. (B) Spreading area of HUVECs. (D) AR definition diagram of cell and nucleus. (E, F) Nucleus aspect ratio and Nuclear shape index calculation. Mean ± standard deviation, n > 40, *p < 0.05, **p < 0.01, ***p < 0.001, ANOVA.

sensors encompass FAK, Paxillin, Vinculin, and Talin, all implicated in cell adhesion and spreading, along with Rac1 and RhoA, which play integral roles in cell cytoskeletal remodeling [42].

PCR results show that under mechanical stretching conditions, there is a significant upregulation in gene expression of talin (Fig. 10A), vinculin (Fig. 10B), and rac1(Fig. 10C), while the expression of FAK (Fig. 10E), paxillin (Fig. 10F), and RhoA (Fig. 10D) does not exhibit a notable increase.

Furthermore, endothelial nitric oxide synthase (eNOS) plays a key role in the NO release pathway. To deepen our understanding of how the cyclic mechanical stimuli influence NO release, we conducted molecular-level detection of eNOS gene expression. The results suggest that, under 10 % strain and 1 Hz cyclic stretching stimulation, the gene expression of eNOS (Fig. 9E) is significantly elevated in cells after 24 hours compared to cells in unstretched conditions , aligning with established research findings [43].

4. Discussion

The design principles for vascular tissue engineering scaffolds prioritize biomimicry to facilitate cell anchoring to the ECM for survival. The electrospinning method is employed to achieve suitable ECM morphology for small-diameter artificial vascular scaffolds [44], utilizing PLCL known for its exceptional biomechanical properties and biocompatibility [45]. Endothelial cells adhere, align, and extend on anisotropic PLCL fiber matrices, responding to mechanical stimuli through alignment in the direction of cyclic strain on a 2D uniform matrix [46,47]. Our research aims to deepen understanding regarding the variation in the morphology and function of endothelial cells under the combined forces of uniaxial cyclic stretching [48].

We successfully obtained three different scaffold membrane morphologies: flat, random, and aligned membranes.The surface stiffness of the electrostatically spun films was close to but higher than that of the planar films, with all three having surface stiffnesses in the range of 6–25 MPa.The increase in stiffness could be attributed to the rapid stretching and rearrangement of the PLCL molecular chains under the action of a high-voltage electric field during the electrospinning process, resulting in a relatively regular arrangement with greater resistance to deformation. In contrast, the molecular chains in planar PLCL films rearrange at a slower rate during solvent evaporation. Nevertheless, the effect of surface stiffness on the cellular response to mechanical stimuli can be ruled out, as the cells perceive stiffness at the kPa level. In addition to the surface stiffness, we also performed a statistical analysis of the fibre diameter and fibre orientation of the electrostatically spun filaments from the Random and Aligned groups, as the surface wettability was already statistically analyzed and showed no significant differences. Prior to the application of mechanical stimuli, all three groups of samples showed good bioactivity and cell proliferation. In particular the electrostatically spun fibres were better than the planar membranes.

Most importantly, the samples exhibited good recovery and stability under mechanical stretching, providing a good platform for further biological experiments. Many tissues and biomaterials exhibit relatively linear elasticity when subjected to small deformations, typically less than 20%. The stress-strain relationship is characterised by a relatively constant slope (referred to as Young's modulus E) [49]. In addition, under physiological conditions, blood vessels undergo cyclic expansion

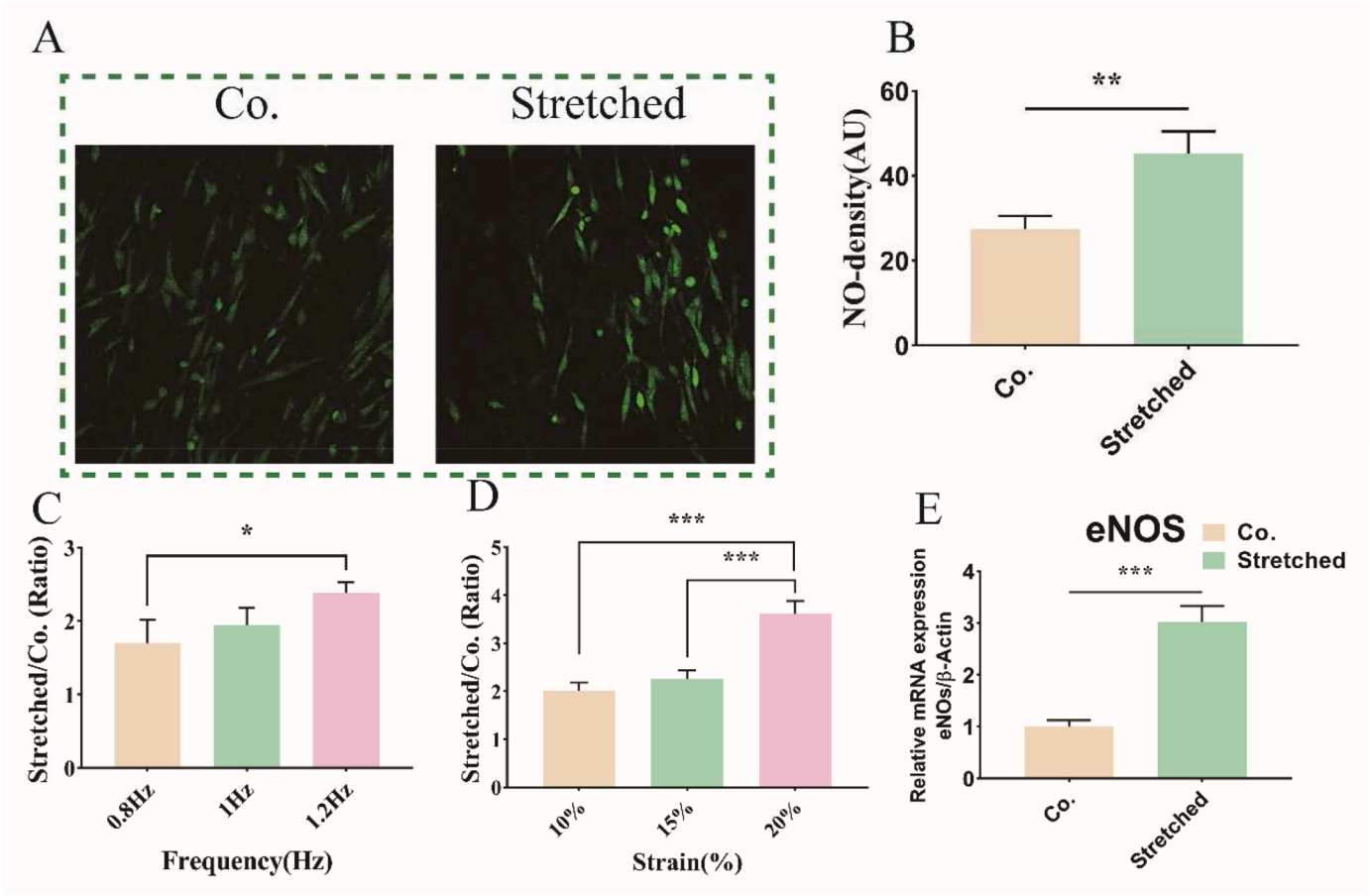

Fig. 9. Immunofluorescence staining and Statistical analysis of NO release. A) DAF-FM staining. B) Laser intensity mean values of NO release under Co.(unstretched) and Stretched. C-D) Stretched/unstretched ratio of NO release in different Frequency and Strain (Reference to formula 5). E) mRNA expressions of the nitric oxide synthase (eNOS) genes related to cell adhesion quantified by q-PCR.

and contraction. Studies have shown that human vascular tissue exhibits circumferential tensile strengths ranging from 0.3 to 3.3 MPa [31]. The circumferential strain during pulsatile blood vessel circulation typically falls within the range of 10–15% [25]. This guided us in setting the frequency of mechanical stimulation and the amount of stretching.

The samples were subjected to uniaxial cyclic dynamic stretching for up to 24 hours to observe the cell response. The shapes of the cells on the different membranes were found to be different. On the flat membrane, the 'anchor points' of the cells were observed to be random, resulting in a random cell shape. In contrast, on the fibrous membrane, the cells were guided by the linear 'anchor points' and polarised in the direction of the fibres. This is consistent with the concept of contact guidance as proposed by Ref. [48]. Mechanical stimulation causes endothelial cell actin fibres to reorganize into stress fibres in the direction of minimum matrix deformation , resulting in cell shrinkage in the stretching direction and repolarisation in the non-stretching direction, consistent with stress avoidance theory [50]. The cell direction on the flat membrane shifted by approximately 40 degrees relative to the stretching direction. In the case of random and aligned fibre membranes, although no obvious rotation was observed, the polarization in the fibre direction was found to be significantly reduced, resulting in the emergence of different orientations (Fig. 7A–C) [51].

Integrin, a key molecule for perceiving mechanical signals from the ECM, transmits these signals to adhesion complexes, triggering the extension and delivery of force sensor proteins [52,53]. These signals guide the aggregation and reorganization of stress fibers, influencing the nuclear localization function of transcription regulatory factors through the LINC complex (Fig. 11) [54,55]. Cyclic stretching increased the expression of talin, vinculin, Rac1(Fig. 10), consistent with the existing studies, while the FAK and Paxillin did not exhibit a significant response [56].The small GTPase Rho and its target Rho kinase (ROCK) are identified as central regulators of endothelial cytoskeletal contractility by increasing MLC phosphorylation to form actin stress fibers [57]. Rac1 is a member of the Rho family of GTPases, which enhances endothelial function by mediating the formation of peripheral F-actin, the expansion of intercellular junctions, and the formation of cell adhesion-associated signaling protein complexes. The physiological stretching forces cause talin to be stretched, thereby exposing cryptic binding sites for vinculin. This, in turn, influences the interaction between talin (a protein that links liganded membrane integrins to the cytoskeleton) and vinculin (an adhesion protein activated by talin binding). This leads to the reorganization of the cytoskeleton. This finding is in accordance with the results of previous studies in this field [58,59].

NO release is crucial in inhibiting thrombus formation in small-diameter vascular grafts and serves as a signaling molecule. Both the magnitude and frequency of uniaxial cyclic strain promote NO release, attributed to the alteration in cell morphology induced by cyclic strain. Spindle-shaped cells exhibit lower NO production compared to cells under circular and non-restricted culture conditions [60].

5. Conclusion

In this study, we investigated the alterations in both the morphological and functional aspects of endothelial cells subjected to uniaxial cyclic stretching within three distinct matrix morphologies. Concurrently, we conducted an in-depth analysis of the mRNA expression levels

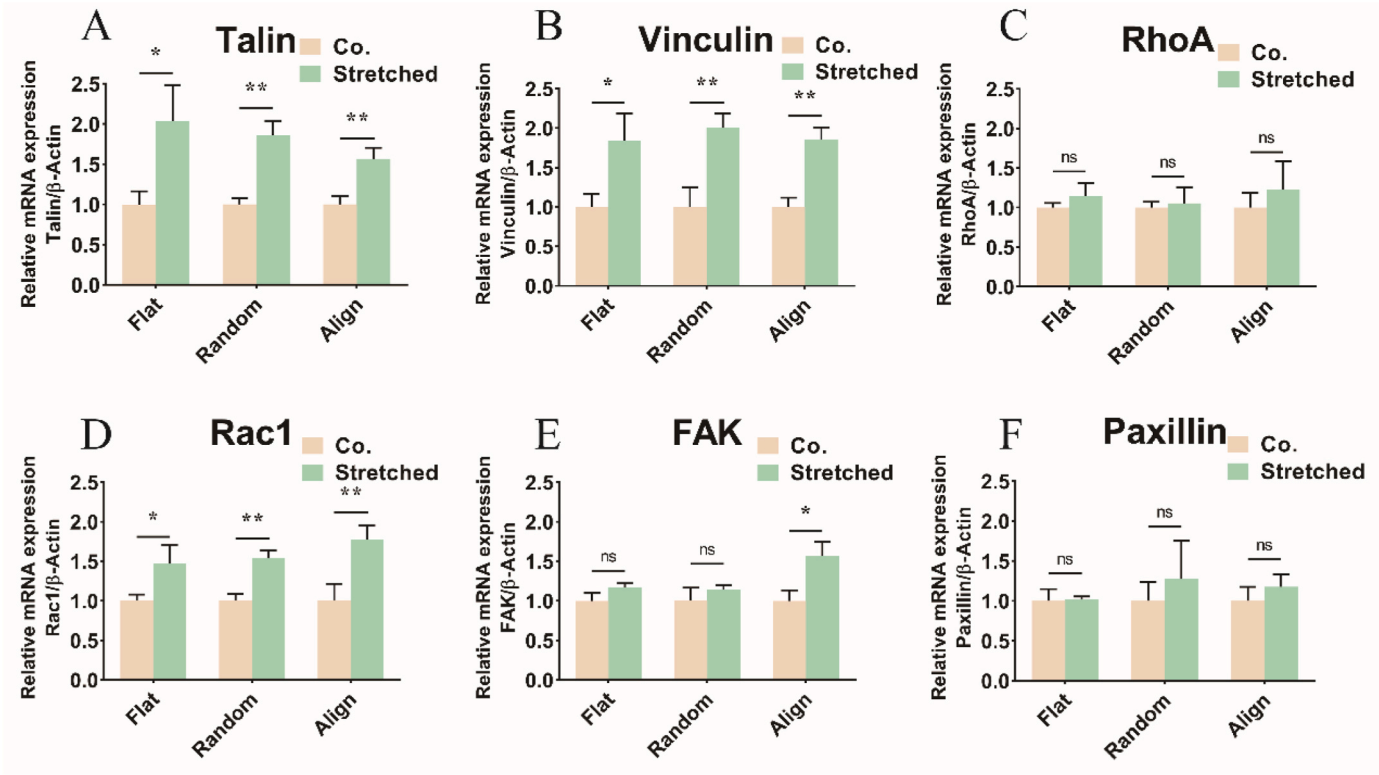

Fig. 10. mRNA expressions of the genes related to dynamic actin rearrangement quantified by q-PCR under Co.(unstretched) and Stretched. (talin, vinculin, RhoA, Rac1,FAK, paxillin). Mean ± standard deviation, *p < 0.05, **p < 0.01, ***p < 0.001, *t*-test.

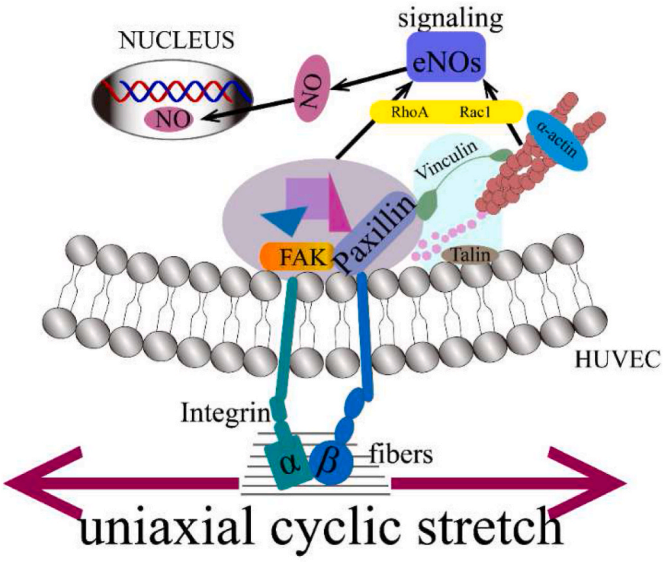

Fig. 11. Cyclic stretching regulates the mechanism of EC mechanical conduction.

of mechanosensitive proteins using PCR technology. Our results elucidated that while uniaxial cyclic stretching has the capacity to reorient cells within isotropic geometric constraints, the anisotropy inherent in the basal morphology remains the primary determinant influencing cell morphology. Additionally, the study revealed that uniaxial cyclic stretching induces the release of NO and establishes a positive correlation with both strain amplitude and strain frequency. Notably, strain amplitude demonstrateed a more pronounced positive effect on NO release in this context.

CRediT authorship contribution statement

Cuihong Ren: Writing – original draft, Methodology, Investigation, Formal analysis, Conceptualization. **Zhonghua Chang:** Validation, Investigation. **Kecheng Li:** Validation, Investigation. **Xiaofeng Wang:** Writing – review & editing, Supervision, Formal analysis, Conceptualization. **Dongfang Wang:** Writing – review & editing. **Yiyang Xu:** Visualization, Investigation. **Xiaomeng Li:** Validation, Investigation. **Qian Li:** Writing – review & editing, Supervision, Project administration, Funding acquisition, Conceptualization.

Declaration of competing interest

The authors declare that they have no known competing financial interests or personal relationships that could have appeared to influence the work reported in this paper.

Data availability

No data was used for the research described in the article.

Acknowledgments

This work was supported by the International Science & Technology Cooperation Program of China (2015DFA30550), the “111” Project of Henan Province, the Science and Technology Research Projects of Henan Province (232102521001).

Appendix A. Supplementary data

Supplementary data to this article can be found online at https://doi.org/10.1016/j.mtbio.2024.101152.

References

[1] E. Gordon, L. Schimmel, M. Frye, The importance of mechanical forces for in vitro endothelial cell Biology, Front. Physiol. 11 (2020), https://doi.org/10.3389/fphys.2020.00684, 684–684.

[2] L. Wang, S. Wu, G. Cao, Y. Fan, N. Dunne, X. Li, Biomechanical studies on biomaterial degradation and co-cultured cells: mechanisms, potential applications, challenges and prospects, J. Mater. Chem. B 7 (2019) 7439–7459, https://doi.org/10.1039/C9TB01539F.

[3] P. Gupta, B.B. Mandal, Tissue-Engineered vascular grafts: emerging Trends and Technologies, Adv. Funct. Mater. 31 (2021) 2100027, https://doi.org/10.1002/adfm.202100027.

[4] Y. Shao, J.M. Mann, W. Chen, J. Fu, Global architecture of the F-actin cytoskeleton regulates cell shape-dependent endothelial mechanotransduction, Integr Biol-Uk 6 (2014) 300–311, https://doi.org/10.1039/c3ib40223a.

[5] N.F. Jufri, A. Mohamedali, A. Avolio, M.S. Baker, Mechanical stretch: physiological and pathological implications for human vascular endothelial cells, Vasc. Cell 7 (2015) 1–12, https://doi.org/10.1186/s13221-015-0033-z.

[6] I. Constantinou, E.E. Bastounis, Cell-stretching devices: advances and challenges in biomedical research and live-cell imaging, Trends Biotechnol. 41 (2023) 939–950, https://doi.org/10.1016/j.tibtech.2022.12.009.

[7] U. Faust, N. Hampe, W. Rubner, N. Kirchgeßner, S. Safran, B. Hoffmann, R. Merkel, Cyclic stress at mHz frequencies aligns Fibroblasts in direction of Zero strain, PLoS One 6 (2011) e28963, https://doi.org/10.1371/journal.pone.0028963.

[8] S. Jungbauer, H. Gao, J.P. Spatz, R. Kemkemer, Two characteristic Regimes in frequency-dependent dynamic reorientation of Fibroblasts on cyclically stretched substrates, Biophys. J. 95 (2008) 3470–3478, https://doi.org/10.1529/biophysj.107.128611.

[9] K. Nagayama, Y. Kimura, N. Makino, T. Matsumoto, Strain waveform dependence of stress fiber reorientation in cyclically stretched osteoblastic cells: effects of viscoelastic compression of stress fibers, American Journal of Physiology-Cell Physiology 302 (2012) C1469–C1478, https://doi.org/10.1152/ajpcell.00155.2011.

[10] A.M. Goldyn, P. Kaiser, J.P. Spatz, C. Ballestrem, R. Kemkemer, The kinetics of force-induced cell reorganization depend on microtubules and actin, Cytoskeleton 67 (2010) 241–250, https://doi.org/10.1002/cm.20439.

[11] V. Gupta, K. Grandeallen, Effects of static and cyclic loading in regulating extracellular matrix synthesis by cardiovascular cells, Cardiovasc. Res. 72 (2006) 375–383, https://doi.org/10.1016/j.cardiores.2006.08.017.

[12] R. Krishnan, E.P. Canović, A.L. Iordan, K. Rajendran, G. Manomohan, A.P. Pirentis, M.L. Smith, J.P. Butler, J.J. Fredberg, D. Stamenović, Fluidization, resolidification, and reorientation of the endothelial cell in response to slow tidal stretches, Am J Physiol-Cell Ph 303 (2012) C368–C375, https://doi.org/10.1152/ajpcell.00074.2012.

[13] B. Avadhanam, V. Gupta, M. Butlin, A. Avolio, Substrate stiffness and frequency of cyclic stretch modulate expression of endothelial nitric oxide synthase in human endothelial cells, J. Hypertens. 37 (2019) e72–e73, https://doi.org/10.1097/01.hjh.0000571092.52214.5d.

[14] Y. Mulla, F. MacKintosh, G.H. Koenderink, Origin of slow stress relaxation in the cytoskeleton, Phys. Rev. Lett. 122 (2019) 218102, https://doi.org/10.1103/physrevlett.122.218102.

[15] I. Andreu, B. Falcones, S. Hurst, N. Chahare, X. Quiroga, A.-L. Le Roux, Z. Kechagia, A.E.M. Beedle, A. Elosegui-Artola, X. Trepat, R. Farré, T. Betz, I. Almendros, P. Roca-Cusachs, The force loading rate drives cell mechanosensing through both reinforcement and cytoskeletal softening, Nat. Commun. 12 (2021) 4229, https://doi.org/10.1038/s41467-021-24383-3.

[16] B. Liu, M.-J. Qu, K.-R. Qin, H. Li, Z.-K. Li, B.-R. Shen, Z.-L. Jiang, Role of cyclic strain frequency in regulating the alignment of vascular smooth muscle cells in vitro, Biophys. J. 94 (2008) 1497–1507, https://doi.org/10.1529/biophysj.106.098574.

[17] R. Kaunas, P. Nguyen, S. Usami, S. Chien, Cooperative effects of Rho and mechanical stretch on stress fiber organization, Proc. Natl. Acad. Sci. USA 102 (2005) 15895–15900, https://doi.org/10.1073/pnas.0506041102.

[18] K. Man, J. Liu, K.M. Phan, K. Wang, J.Y. Lee, X. Sun, M. Story, D. Saha, J. Liao, H. Sadat, Y. Yang, Dimensionality-dependent mechanical stretch regulation of cell behavior, Acs Appl Mater Inter 14 (2022) 17081–17092, https://doi.org/10.1021/acsami.2c01266.

[19] S. Wang, X. Mo, Jiang, Gao, Qiu, Zhuang, Wang, Fabrication of small-diameter vascular scaffolds by heparin-bonded P(LLA-CL) composite nanofibers to improve graft patency, Int. J. Nanomed. (2013) 2131, https://doi.org/10.2147/IJN.S44956.

[20] H. Kuang, Y. Wang, Y. Shi, W. Yao, X. He, X. Liu, X. Mo, S. Lu, P. Zhang, Construction and performance evaluation of Hep/silk-PLCL composite nanofiber small-caliber artificial blood vessel graft, Biomaterials 259 (2020) 120288, https://doi.org/10.1016/j.biomaterials.2020.120288.

[21] S. Tara, H. Kurobe, M.W. Maxfield, K.A. Rocco, T. Yi, Y. Naito, C.K. Breuer, T. Shinoka, Evaluation of remodeling process in small-diameter cell-free tissue-engineered arterial graft, J. Vasc. Surg. 62 (2015) 734–743, https://doi.org/10.1016/j.jvs.2014.03.011.

[22] M. Zhu, Y. Wu, W. Li, X. Dong, H. Chang, K. Wang, P. Wu, J. Zhang, G. Fan, L. Wang, Biodegradable and elastomeric vascular grafts enable vascular remodeling, Biomaterials 183 (2018) 306–318, https://doi.org/10.1016/j.biomaterials.2018.08.063.

[23] Z. Niu, X. Wang, X. Meng, X. Guo, Y. Jiang, Y. Xu, Q. Li, C. Shen, Controllable fiber orientation and nonlinear elasticity of electrospun nanofibrous small diameter tubular scaffolds for vascular tissue engineering, Biomed Mater 14 (2019) 035006, https://doi.org/10.1088/1748-605X/ab07f1.

[24] X. Li, X. Wang, D. Yao, J. Jiang, X. Guo, Y. Gao, Q. Li, C. Shen, Effects of aligned and random fibers with different diameter on cell behaviors, Colloid Surface B 171 (2018) 461–467, https://doi.org/10.1016/j.colsurfb.2018.07.045.

[25] M.A. Anwar, J. Shalhoub, C.S. Lim, M.S. Gohel, A.H. Davies, The effect of pressure-induced mechanical stretch on vascular Wall differential gene expression, J. Vasc. Res. 49 (2012) 463–478.

[26] J. Schindelin, I. Arganda-Carreras, E. Frise, V. Kaynig, M. Longair, T. Pietzsch, S. Preibisch, C. Rueden, S. Saalfeld, B. Schmid, Fiji: an open-source platform for biological-image analysis, Nat. Methods 9 (2012) 676–682, https://doi.org/10.1038/nmeth.2019.

[27] M. Hart, J. Lauer, M. Selig, M. Hanak, B. Walters, B. Rolauffs, Shaping the cell and the Future: Recent Advancements in Biophysical aspects relevant to regenerative medicine, JFMK 3 (2017) 2, https://doi.org/10.3390/jfmk3010002.

[28] M. Versaevel, T. Grevesse, S. Gabriele, Spatial coordination between cell and nuclear shape within micropatterned endothelial cells, Nat. Commun. 3 (2012) 671, https://doi.org/10.1038/ncomms1668.

[29] Y. Zhang, X. Wang, Y. Zhang, Y. Liu, D. Wang, X. Yu, H. Wang, Z. Bai, Y. Jiang, X. Li, W. Zheng, Q. Li, Endothelial cell migration regulated by surface topography of poly(ε-caprolactone) nanofibers, Acs Biomater Sci Eng 7 (2021) 4959–4970, https://doi.org/10.1021/acsbiomaterials.1c00951.

[30] M.B. Taskin, D. Xia, F. Besenbacher, M. Dong, M. Chen, Nanotopography featured polycaprolactone/polyethyleneoxide microfibers modulate endothelial cell response, Nanoscale 9 (2017) 9218–9229, https://doi.org/10.1039/c7nr03326e.

[31] B.A. Hamedani, M. Navidbakhsh, H.A. Tafti, Comparison between mechanical properties of human saphenous vein and umbilical vein, Biomed. Eng. Online 11 (2012) 59, https://doi.org/10.1186/1475-925X-11-59.

[32] C.J. van Andel, P.V. Pistecky, C. Borst, Mechanical properties of porcine and human arteries: implications for coronary anastomotic connectors, Ann. Thorac. Surg. 76 (2003) 58–64, https://doi.org/10.1016/S0003-4975(03)00263-7.

[33] Y. Zheng, B.J. Thelen, N. Rajaram, V.N. Krishnamurthy, J. Hamilton, M.A. Funes-Lora, T. Morgan, L. Yessayan, B. Bishop, N. Osborne, P. Henke, A.J. Shih, W. F. Weitzel, Angioplasty induced changes in Dialysis vascular access Compliance, Ann. Biomed. Eng. 49 (2021) 2635–2645, https://doi.org/10.1007/s10439-021-02844-6.

[34] S. Müller, M. Ueda, T. Isoshima, T. Ushida, Y. Ito, Stretching of fibroblast cells on micropatterned gelatin on silicone elastomer, J. Mater. Chem. B 8 (2020) 416–425, https://doi.org/10.1039/C9TB02203A.

[35] J. Aureille, N. Belaadi, C. Guilluy, Mechanotransduction via the nuclear envelope: a distant reflection of the cell surface, Curr. Opin. Cell Biol. 44 (2017) 59–67, https://doi.org/10.1016/j.ceb.2016.10.003.

[36] A.B.C. Buskermolen, H. Suresh, S.S. Shishvan, A. Vigliotti, A. DeSimone, N. A. Kurniawan, C.V.C. Bouten, V.S. Deshpande, Entropic forces drive cellular contact guidance, Biophys. J. 116 (2019) 1994–2008, https://doi.org/10.1016/j.bpj.2019.04.003.

[37] J.O. Lundberg, E. Weitzberg, Nitric oxide signaling in health and disease, Cell 185 (2022) 2853–2878, https://doi.org/10.1016/j.cell.2022.06.010.

[38] A. Jannatbabaei, M. Tafazzoli-Shadpour, E. Seyedjafari, Effects of substrate mechanics on angiogenic capacity and nitric oxide release in human endothelial cells, Ann Ny Acad Sci 1470 (2020) 31–43, https://doi.org/10.1111/nyas.14326.

[39] W.M. Kuebler, U. Uhlig, T. Goldmann, G. Schael, A. Kerem, K. Exner, C. Martin, E. Vollmer, S. Uhlig, Stretch Activates nitric oxide production in Pulmonary vascular endothelial cells in Situ, Am. J. Respir. Crit. Care Med. 168 (2003) 1391–1398, https://doi.org/10.1164/rccm.200304-562OC.

[40] J.-L. Balligand, O. Feron, C. Dessy, eNOS activation by physical forces: from short-Term regulation of contraction to Chronic remodeling of cardiovascular tissues, Physiol. Rev. 89 (2009) 481–534, https://doi.org/10.1152/physrev.00042.2007.

[41] M.J. Davis, S. Earley, Y.-S. Li, S. Chien, Vascular mechanotransduction, Physiol. Rev. 103 (2023) 1247–1421.

[42] M.R. Chastney, J.R.W. Conway, J. Ivaska, Integrin adhesion complexes, Curr. Biol. 31 (2021) R536–R542, https://doi.org/10.1016/j.cub.2021.01.038.

[43] K.A. Mohammed, N. Nasreen, R.S. Tepper, V.B. Antony, Cyclic stretch induces PlGF expression in bronchial airway epithelial cells via nitric oxide release, Am. J. Physiol. Lung Cell Mol. Physiol. 292 (2007) L559–L566, https://doi.org/10.1152/ajplung.00075.2006.

[44] Q. Jin, Y. Fu, G. Zhang, L. Xu, G. Jin, L. Tang, J. Ju, W. Zhao, R. Hou, Nanofiber electrospinning combined with rotary bioprinting for fabricating small-diameter vessels with endothelium and smooth muscle, Compos. B Eng. 234 (2022) 109691, https://doi.org/10.1016/j.compositesb.2022.109691.

[45] Y. Wang, G. Li, L. Yang, R. Luo, G. Guo, Development of Innovative biomaterials and devices for the treatment of cardiovascular diseases, Adv. Mater. 34 (2022) 2201971, https://doi.org/10.1002/adma.202201971.

[46] C. Natale, J. Lafaurie-Janvore, M. Ventre, A. Babataheri, A. Barakat, Focal adhesion clustering drives endothelial cell morphology on patterned surfaces, Journal of the Royal Society Interface 16 (2019) 20190263, https://doi.org/10.1098/rsif.2019.0263.

[47] T. Jiang, E.J. Carbone, K.W.-H. Lo, C.T. Laurencin, Electrospinning of polymer nanofibers for tissue regeneration, Prog. Polym. Sci. 46 (2015) 1–24, https://doi.org/10.1016/j.progpolymsci.2014.12.001.

[48] A. Ippolito, V.S. Deshpande, Contact guidance via heterogeneity of substrate elasticity, Acta Biomater. 163 (2023) 158–169, https://doi.org/10.1016/j.actbio.2021.11.024.

[49] C. Storm, J.J. Pastore, F.C. MacKintosh, T.C. Lubensky, P.A. Janmey, Nonlinear elasticity in biological gels, Nature 435 (2005) 191–194, https://doi.org/10.1038/nature03521.

[50] W.C. Aird, Phenotypic heterogeneity of the endothelium: I. Structure, function, and mechanisms, Circ. Res. 100 (2007) 158–173, https://doi.org/10.1161/01.res.0000255691.76142.4a.
[51] P. Sipkema, P.J. van der Linden, N. Westerhof, F.C. Yin, Effect of cyclic axial stretch of rat arteries on endothelial cytoskeletal morphology and vascular reactivity, J. Biomech. 36 (2003) 653–659, https://doi.org/10.1016/s0021-9290(02)00443-8.
[52] A. Elosegui-Artola, R. Oria, Y. Chen, A. Kosmalska, C. Pérez-González, N. Castro, C. Zhu, X. Trepat, P. Roca-Cusachs, Mechanical regulation of a molecular clutch defines force transmission and transduction in response to matrix rigidity, Nat. Cell Biol. 18 (2016) 540–548, https://doi.org/10.1038/ncb3336.
[53] M. Yao, B.T. Goult, H. Chen, P. Cong, M.P. Sheetz, J. Yan, Mechanical activation of vinculin binding to talin locks talin in an unfolded conformation, Sci. Rep. 4 (2014) 4610, https://doi.org/10.1038/srep04610.
[54] T.J. Kirby, J. Lammerding, Emerging views of the nucleus as a cellular mechanosensor, Nat. Cell Biol. 20 (2018) 373–381, https://doi.org/10.1038/s41556-018-0038-y.
[55] A. Tajik, Y. Zhang, F. Wei, J. Sun, Q. Jia, W. Zhou, R. Singh, N. Khanna, A. S. Belmont, N. Wang, Transcription upregulation via force-induced direct stretching of chromatin, Nature Mater 15 (2016) 1287–1296, https://doi.org/10.1038/nmat4729.
[56] N. Zebda, O. Dubrovskyi, K.G. Birukov, Focal adhesion kinase regulation of mechanotransduction and its impact on endothelial cell functions, Microvasc. Res. 83 (2012) 71–81, https://doi.org/10.1016/j.mvr.2011.06.007.
[57] K.G. Birukov, V.N. Bochkov, A.A. Birukova, K. Kawkitinarong, A. Rios, A. Leitner, A.D. Verin, G.M. Bokoch, N. Leitinger, J.G.N. Garcia, Epoxycyclopentenone-containing oxidized phospholipids restore endothelial barrier function via Cdc42 and Rac, Circ. Res. 95 (2004) 892–901.
[58] C.J. Bettinger, R. Langer, J.T. Borenstein, Engineering substrate topography at the micro- and nanoscale to control cell function, Angew. Chem. Int. Ed. 48 (2009) 5406–5415, https://doi.org/10.1002/anie.200805179.
[59] A. del Rio, R. Perez-Jimenez, R. Liu, P. Roca-Cusachs, J.M. Fernandez, M.P. Sheetz, Stretching Single talin Rod molecules Activates vinculin binding, Science 323 (2009) 638–641, https://doi.org/10.1126/science.1162912.
[60] S. Kidoaki, T. Matsuda, Shape-engineered vascular endothelial cells: nitric oxide production, cell elasticity, and actin cytoskeletal features, J. Biomed. Mater. Res. 81A (2007) 728–735, https://doi.org/10.1002/jbm.a.31112.